

PCCP

Accepted Manuscript



This article can be cited before page numbers have been issued, to do this please use: R. P. Ribeiro, E. Longo, J. Andrés and S. R. R. de Lazaro, *Phys. Chem. Chem. Phys.*, 2018, DOI: 10.1039/C8CP04443K.



This is an Accepted Manuscript, which has been through the Royal Society of Chemistry peer review process and has been accepted for publication.

Accepted Manuscripts are published online shortly after acceptance, before technical editing, formatting and proof reading. Using this free service, authors can make their results available to the community, in citable form, before we publish the edited article. We will replace this Accepted Manuscript with the edited and formatted Advance Article as soon as it is available.

You can find more information about Accepted Manuscripts in the [author guidelines](#).

Please note that technical editing may introduce minor changes to the text and/or graphics, which may alter content. The journal's standard [Terms & Conditions](#) and the ethical guidelines, outlined in our [author and reviewer resource centre](#), still apply. In no event shall the Royal Society of Chemistry be held responsible for any errors or omissions in this Accepted Manuscript or any consequences arising from the use of any information it contains.

1 **A DFT investigation of the role of oxygen vacancies on the structural, electronic**
2 **and magnetic properties of ATiO₃ (A = Mn, Fe, Ni) multiferroic materials**

3 R. A. P. Ribeiro¹, E. Longo², J. Andrés^{3,*}, S. R. de Lazaro¹

4 ¹*Department of Chemistry, State University of Ponta Grossa, Av. General Carlos Cavalcanti,*
5 *4748, 84030-900, Ponta Grossa, PR, Brazil*

6 ²*CDMF-UFSCar, Universidade Federal de São Carlos, PO Box 676, 13565-905 São Carlos,*
7 *SP, Brazil*

8 ³*Department of Physical and Analytical Chemistry, University Jaume I (UJI), Castelló 12071,*
9 *Spain*

10 **Corresponding author; Email address: andres@qfa.uji.es*

11
12 **ABSTRACT**

13 In order to achieve deep insight into the multiferroic behavior and electronic properties
14 of intrinsic oxygen vacancies in ATiO₃ (A = Mn, Fe, Ni), first-principles calculations
15 based on hybrid density functional theory were carried out for bulk and non-polar (110)
16 surface models. We found that the formation of an oxygen vacancy is accompanied by
17 structural and electronic disorders in the constituent clusters of [TiO₆] and [AO₆] in
18 ATiO₃, that become [TiO₅] and [AO₅], respectively. This perturbation contributes to the
19 generation of intermediary energy levels in the band gap region, thus narrowing the
20 required excitation energy. In addition, the remaining electrons are mainly trapped in
21 the empty 3d orbitals of the Ti cations neighboring the oxygen vacancy, generating
22 [TiO₅][•] (3d¹) that mediates an antiferromagnetic to ferromagnetic transition in MnTiO₃
23 and FeTiO₃ materials. In particular, MnTiO₃ surfaces show exposed [TiO₄][•] species that
24 are responsible for its half-metallic behavior. The present work provides compelling
25 evidence that controlling oxygen vacancies can be a valuable strategy to tailor the
26 multiferroic properties of ATiO₃ materials.

27
28 **Key-words:** Oxygen vacancies, magnetism, multiferroic properties, magnetic coupling,
29 spin density.

30 1. Introduction

31 Multiferroic materials are capable of combining different ferroic properties
32 (magnetism, ferroelectricity, and elasticity) and have attracted a large amount of
33 scientific attention due to their technological applications, mainly in the electronics
34 industry.¹⁻³ In particular, ABO₃-type materials are widely investigated for technological
35 purposes, such as ferroelectric devices, gas sensors, actuators and others, because they
36 can display a variety of physical and chemical properties depending on the metal atoms
37 occupying the A and B-sites⁴. Therefore, new multiferroic materials can be synthesized
38 based on this class of compounds. For instance, ilmenite-based ATiO₃ (A = Mn, Fe, Co,
39 Ni) materials have been widely studied for their intriguing magnetoelectric effects.⁵⁻¹⁵

40 In previous studies of this class of compounds, we noted that changes in both the
41 A- and B-site cations induce structural and electronic distortions that drastically modify
42 their magnetic and electrical behaviors, which are the main targets of multiferroic
43 materials design.¹⁶⁻¹⁸ An alternative method of inducing these distortions in solid state
44 materials relies on the presence of oxygen vacancies (V_O). This type of defect is
45 common in metallic oxides due to the crystal growth process, annealing, or substitutions
46 inside the crystalline structure leading to electronic defects (excess electrons or holes)
47 that can modify several features (structural, optical, electrical, magnetic, and others) of
48 solid state materials.¹⁹ Recently, theoretical and experimental studies have determined
49 that oxygen vacancies play a fundamental role in tuning the optical, electrical, and
50 magnetic properties of oxides.²⁰⁻²⁶ For instance, Pacchioni *et al.* described
51 ferromagnetism in reduced ZrO_{2-x} nanoparticles and indicated that neutral oxygen
52 vacancies can induce local ferromagnetism in non-magnetic 4d cations through a
53 ferromagnetic arrangement between reduced Zr³⁺ centers.^{27, 28} The same authors also

54 predicted local magnetism in other materials such as WO_3 , TiO_2 , and NiO by using both
55 bulk and surface models.^{29,30} However, it is important to point out that the existence of
56 reduced centers does not guarantee the existence of ferromagnetism, because the spins
57 located at the reduced centers could be antiparallel ordered, as reported for TiO_2 .³¹

58 It is widely recognized that ferromagnetic-ferroelectric (FEM-FE) behavior is
59 more desirable than antiferromagnetic-ferroelectric (AFM-FE) behavior for multiferroic
60 applications.^{32,33} In this context, the presence of V_{O} is crucial because it can generate
61 FEM ordering in AFM-FE materials. This fact can be ascribed to the partially disturbed
62 (super-)exchange interactions between magnetic ions caused by bond breaking
63 processes closer to the defect, as well as the excess charge or holes due to local non-
64 stoichiometry altering the valence number of magnetic or non-magnetic ions near the
65 vacancy, which leads to a change in the local magnetic moment.³⁴ Such a mechanism
66 has been successfully applied to generate ferromagnetic ordering in common
67 ferroelectric perovskite materials, such as BaTiO_3 , SrTiO_3 , and PbTiO_3 , thus enabling
68 them to exhibit magnetoelectric coupling.^{21,26,35-38} In addition, Li and co-authors have
69 reported that the presence of V_{O} controls magnetism and ferroelectric ordering,
70 demonstrating that oxygen vacancies create $[\text{TiO}_5]'$ ($3d^1$) defect states, mediating the
71 ferromagnetic coupling between the localized Eu ($4f^7$) spins, and increase the off-center
72 displacement of Ti cations, enhancing the ferroelectric order.^{39,40} Similar results were
73 found by Cheng *et al.* and Deng *et al.* for YMnO_3 multiferroic materials using both
74 experimental techniques and theoretical calculations.^{41,42}

75 Experimental and theoretical studies have been developed to elucidate the role of
76 defects on the multiferroic properties of BiFeO_3 , the most studied single-phase
77 multiferroic material, which has a high ferroelectric Curie temperature ($T_c = 1103 \text{ K}$)

78 and antiferromagnetic Neel temperature ($T_N = 643$ K).^{43, 44} More recently, Rojac *et al.*⁴⁵
79 reported atomic-scale chemical and structural analyses showing that the accumulation of
80 charged defects at domain walls in BiFeO₃ provided superior electrical properties for the
81 samples, an observation that was confirmed by Schrade *et al.*^{45, 46} On the other hand,
82 focusing on the defect-driven antiferromagnetic-ferromagnetic transition, Wu *et al.*
83 noted an unusual ferromagnetism in samples synthesized with low-temperature, fast,
84 solid-state reactions, which was attributed to the presence of oxygen-deficient centers
85 that suppress the spin circular cycloid in BiFeO₃.⁴⁷ Further, several theoretical studies
86 have confirmed such predictions, showing that oxygen vacancies affect the magnetic
87 moments at neighboring Fe ions. These vacancies, along with additional ferroelectric
88 polarizations due to the cation displacement, provide the rich variety of multiferroic
89 behaviors observed in BiFeO₃ based on the concentration and charge of defect states.^{34,}
90 48-50

91 Transition metal titanates ATiO₃ (A = Mn, Fe, Ni), with LiNbO₃-type (R3c)
92 ilmenite structure, are one of the most promising types of multiferroic materials due to
93 their remarkable magneto-electric coupling. These compounds are structurally
94 isomorphic to BiFeO₃ except that the positions of the A and B cations are exchanged.^{9,}
95 ⁵¹ In the past few years, scientific interest in such materials has increased due to the
96 possibility of controlling their magnetic behavior based on antisymmetric
97 Dzyaloshinskii-Moriya interactions.^{8, 9, 12-14} The R3c structure consists of oxygen layers
98 in a distorted hexagonal close-packed configuration, where the octahedral sites, i.e.
99 [AO₆] and [TiO₆] clusters, are equally occupied by A and Ti cations, respectively. The
100 magneto-electric properties are associated with the presence of A-site cations displaced
101 from the central positions of the oxygen octahedral cages, i.e. [AO₆] clusters, resulting in

102 a spontaneous polarization along the (001) direction^{51, 52} summed to a G-type
103 antiferromagnetic order along (111) planes. Despite current theoretical studies
104 developed for ATiO₃ (A = Mn, Fe, Ni) materials, the role of oxygen vacancies in the
105 intrinsic physical and chemical properties remains unclear.⁸⁻¹⁴

106 In this study, first-principles hybrid density functional theory (DFT) calculations
107 were performed to provide a deep insight into the multiferroic nature and electronic
108 properties of intrinsic point defects in ATiO₃ (A = Mn, Fe, Ni). In this article, the main
109 goal is to show how the generation of oxygen-deficient centers perturbs the exchange-
110 coupling constant between magnetic atoms and induces the formation of magnetic
111 [TiO₅][•] (3d¹) species that contribute to the AFM-FE magnetic transition. These oxygen-
112 deficient centers provide a general interpretation, at the atomic level, of the changes in
113 the magnetic and electronic properties allowing us to elucidate the role of oxygen
114 vacancies in the multiferroic properties of these materials.

115 This article is organized into three further sections. The computational
116 methodology used in this study is described in the following section. The third section,
117 where the results are presented and discussed, is divided into two main subsections. The
118 first one discusses the properties of the bulk ATiO₃ (A = Mn, Fe, Ni) compounds. The
119 second subsection deals with the non-polar (110) surfaces. The last section summarizes
120 the main results of this work.

121

122 2. Computational Methodology

123 DFT calculations were performed using the linear combination of atomic
124 orbitals approach as implemented in the CRYSTAL14 code.⁵³ The A, Ti, and O atoms
125 were described by atom centered all-electron Gaussian basis sets such as 86-411d41G,

126 86-411(d31)G, and 8-411G, respectively.⁵⁴⁻⁵⁶ In all calculations, a PBE0⁵⁷ hybrid
127 functional was adopted for the treatment of exchange and correlation due to its good
128 agreement with the experimental values of many properties computed previously for
129 pristine ATiO₃ (A = Mn, Fe, Ni) multiferroic materials.¹⁸ The analyses of electronic
130 properties by means of density of states, band structure profiles, and electron density
131 distributions were carried out with the new functionalities for property evaluation
132 available in the new version of CRYSTAL (2017).⁵⁸

133 The pristine *R3c* unit cell was computed using a rhombohedral primitive unit
134 cell that contains two ATiO₃ unit formulas (10-atoms) with A (A = Mn, Fe, Ni), Ti and
135 O atoms located at (0, 0, u), (0, 0, 0) and (x, y, z), respectively.^{8, 12, 14} The V_O vacancy
136 was modeled in embedded 2 x 2 x 2 ATiO₃ supercells, containing 80-atoms which
137 corresponds to a defect concentration of 2.1%, as represented in Figure 1. In addition,
138 we considered the creation of oxygen vacancies in non-polar (110) surfaces of ATiO₃
139 materials. This surface was previously found to be the most stable cleavage plane for
140 MnTiO₃, dominating the ideal morphology.⁵⁹ In this case, a 2 x 1 supercell (80-atoms)
141 was used considering three different vacancy configurations (V₁₋₃) due to the existence
142 of three non-equivalent oxygen atoms along the surface plane. The first one (V₁)
143 correspond to a superficial two-fold oxygen atom coordinated with A (A = Mn, Fe, Ni)
144 and Ti cations, while V₂ and V₃ correspond to a superficial three-fold oxygen atom,
145 surrounded by two Ti and one Mn cation in the V₂ case, or coordinated with two Mn
146 and one Ti cation in the V₃ case, as presented in Figure 1.

147

Figure 1

148 Electronic integration over the Brillouin Zone was performed using an 8 x 8 x 8
149 Monkhorst–Pack⁶⁰ k -mesh for the 10-atom unit cell containing 65 k -points. For
150 supercell expansions, a reduced k -mesh density (2 x 2 x 2) was employed containing 8
151 k -points, as was performed by Bjørheim *et al.* to investigate defective BaZrO₃.⁶¹The
152 thresholds controlling the accuracy of the Coulomb and exchange integral calculations
153 were controlled by five thresholds set to 8, 8, 8, 8, and 16. The convergence criteria for
154 mono- and bielectronic integrals were set to 10⁻⁸ Hartree, while the RMS gradient, RMS
155 displacement, maximum gradient and maximum displacement were set to 3 x 10⁻⁵, 1.2 x
156 10⁻⁴, 4.5 x 10⁻⁵ and 1.8 x 10⁻⁴ a.u., respectively.

157 Following the Kroger–Vink notation,⁶² the V_O can be neutral (V_O^x), single-
158 (V_O^\bullet), or double-positively ($V_O^{\bullet\bullet}$) charged, resulting in different mechanisms associated
159 with the trapping of holes at the vacancy sites. Usually, the V_O^x originates from a
160 diamagnetic ($\uparrow\downarrow$) center, which can be transformed into a positively charged vacancy by
161 trapping a hole, while the remaining electron is trapped on the empty states of
162 neighboring metal centers, resulting in a paramagnetic species (\uparrow). In addition, one may
163 expect that further ionization of V_O^\bullet sites could produce double-positively charged $V_O^{\bullet\bullet}$
164 centers, with null magnetic moment. However, the existence of oxygen anions (O²⁻)
165 requires a significant local structural relaxation in order to balance the electron density
166 of the neighboring under-coordinated cations. In this study, only neutral V_O^x species
167 were considered due to the complexity of dealing with charged supercell models in the
168 CRYSTAL code. Here, it is important to point out that the states of a vacancy site are
169 present due to the treatment performed with the CRYSTAL code through GHOST,
170 where the nuclear charge is removed while the Gaussian basis sets are maintained.

171 Experimental results suggest a G-type antiferromagnetic ground-state for all
172 ATiO_3 ($A = \text{Mn, Fe, Ni}$) materials consisting of spins ferromagnetically ordered within
173 (111) planes, while the adjacent planes are antiferromagnetically coupled. In our
174 calculations, lattice parameters and atomic positions were relaxed for both pristine and
175 oxygen-defective models in FEM configuration. Additional single point calculations
176 were performed to ascertain the magnetic ground-state for oxygen-defective supercells
177 due to the remaining two electrons related to the presence of neutral V_O^x centers in the
178 lattice. For this purpose, we considered two collinear magnetic configurations: (i) G-
179 type AFM with two remaining electrons from V_O^x in a singlet closed-shell configuration
180 (AFM-S); (ii) G-type AFM configuration with two remaining electrons from V_O^x in a
181 triplet closed-shell configuration (AFM-T). In addition, the magnetic exchange coupling
182 constant between the two magnetic A^{2+} cations neighboring the V_O^x was analyzed by
183 means of an additional model containing the aftermentioned magnetic clusters in a
184 parallel spin orientation (FIM), keeping the remaining electrons from V_O^x in the
185 previously determined ground-state (AFM-S or AFM-T).

186

187 **3. Results and Discussion**

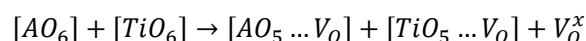
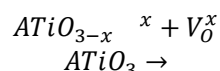
188 *3.1. Bulk*

189 Firstly, the local structural and electronic disorders originating from the presence
190 of oxygen vacancies in ATiO_3 ($A = \text{Mn, Fe, Ni}$) materials were investigated by
191 comparing the structural parameters (unit cell lattice parameters, atom displacement and
192 bond distances for the clusters centered on both A and Ti cations) for pristine and
193 defective transition metal titanates, as summarized in Table 1. The rhombohedral setting

194 was used due to the supercell expansion of the primitive unit cell for oxygen defective
195 systems.

196 **Table 1**

197 An analysis of the results presented in the Table 1 clearly indicates that oxygen
198 vacancies cause singular effects in the crystalline structure of ATiO₃ materials. In
199 general, the creation of oxygen vacancies induces a small volume contraction
200 accompanied by slight distortion of the unit cell, as defective MnTiO₃ and
201 FeTiO₃ models exhibit a lower symmetry ($a \neq b \neq c$ and $\alpha \neq \beta \neq \gamma$) than pristine ones.
202 Additionally, a small distortion was detected for both metal centered clusters closer to
203 the oxygen vacancy that arises from cationic and anionic displacements outward and
204 toward V_O^x , respectively. This relaxation leads to the formation of two different [TiO₅]
205 and [MnO₅] clusters, changing the local symmetries from prismatic D_{3h} [MO₆] clusters
206 in the pristine unit cell to distorted square pyramidal [MO₅] units in the defective model,
207 following the equations:



208 In addition, the creation of oxygen vacancies leads to a new electron density
209 distribution along the metal centered clusters due to the perturbation of the repulsive
210 and attractive forces acting on the A-O and Ti-O chemical bonds. Moreover, this
211 structural distortion can generate intermediary energy levels in the electronic structures
212 of ATiO₃ systems; this is a fundamental key to tuning the magnetic, ferroelectric, and
213 electronic properties of such materials.

214 Aiming to describe the electron density redistribution in the vicinity of the
215 oxygen vacancy, Hirshfeld-I analysis was performed. This kind of analysis has shown

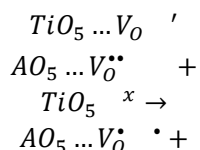
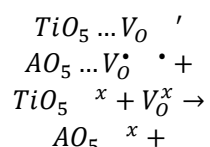
216 very good results for different classes of materials in comparison to Bader's analysis
217 (QTAIM), but at a significantly lower computational cost.⁵⁸

218 **Table 2**

219 In Table 2 the values of the Hirshfeld-I charges and spin densities of both Ti and
220 A centers are reported for both pristine and oxygen deficient ATiO₃. An analysis of the
221 results shows that neutral oxygen vacancies induce a decrease in the positive charge on
222 the metal neighbors and a new electron density distribution of the remaining two
223 electrons, which become delocalized along the [MO₅] and [TiO₅] clusters. Indeed, it
224 was observed that defective MnTiO₃ and FeTiO₃ exhibit a higher charge reduction for
225 Ti cations in comparison to A cations (A = Mn, Fe), whereas defective NiTiO₃ behaves
226 in an opposite way (larger reduction for Ni atoms than for Ti). Therefore, it is possible
227 to argue that [NiO₅] clusters favor electron density redistribution along the Ni-O-Ni
228 framework to a large extent compared to [MnO₅] and [FeO₅], where the remaining
229 electron density is mainly concentrated in the Ti-O-Ti moiety. These results are
230 supported by the QTAIM analysis performed in our previous work for pristine ATiO₃
231 (A = Mn, Fe, Ni), where a higher covalent character for A–O bonds was observed when
232 moving from Mn to Ni due to the increased bond critical path (BCP) electron density,
233 derived from the extended 3d–2p overlap, mainly for the Ni-O bond.¹⁸

234 Therefore, using the electronic parameters evaluated by means of Hirshfeld
235 analysis we can describe the electron localization in the vicinity of the vacancy using
236 the Kroger–Vink notation for defect equations. This method is helpful to clarify the
237 nature of electron-hole localization in the constituent clusters inside the crystalline
238 structure, providing an atomic level point of view of the fundamental mechanism
239 associated with electron excitation and localization which are responsible for many

240 phenomena, such as photoluminescence and photocatalysis.⁶³⁻⁶⁶ In this formalism, the
 241 charge accumulation mechanism could be described as follows using the neutral
 242 $[\text{MO}_n]^x$, positively charged $[\text{MO}_n\text{V}_O^\bullet]^+$, and negatively charged $[\text{MO}_n]'$ cluster notation:
 243



244
 245 Therefore, the results presented in Table 2 suggest the existence of a reduced Ti
 246 species $[\text{TiO}_5]'$ with non-zero magnetic moment resulting from electron trapping, as has
 247 also been observed for other defective Ti-based materials.^{21, 26, 38, 39, 67, 68} In this context,
 248 we argue that the magnetic properties of ATiO_3 materials can be changed by defects due
 249 to an electron resonance between V_O^x that becomes V_O^\bullet and $\text{V}_O^{\bullet\bullet}$, resulting in electron
 250 trapping at the empty 3d energy levels of Ti. This mechanism corresponds to an
 251 alternative and innovative point of view based on atomic-level simulations used to
 252 describe the nature of magnetic properties associated with the presence of vacancies.

253 In order to evaluate the effect of oxygen vacancies on the local and global
 254 magnetic ordering of ATiO_3 (A = Mn, Fe, Ni) compounds, different arrangements of
 255 spin-density alignment were considered. First of all, it was observed that all regular
 256 magnetic clusters $[\text{AO}_6]$ (A = Mn, Fe, Ni) maintain the G-type antiferromagnetic
 257 ordering observed for the pristine bulk material.¹⁸ In addition, in all cases it was

258 observed that the singlet configuration is the most stable arrangement of the remaining
259 two electrons (V_{δ}^x). However, the local spin arrangement in the vicinity of the V_{δ}^x center
260 shows a distinct ordering moving from Mn to Ni.

261 For MnTiO_3 , the obtained results indicate that FIM ordering is 9.8 meV lower in
262 energy than the G-type AFM model. For FeTiO_3 as well, a relative energy difference of
263 around 6.7 meV was observed in comparison to the AFM model. In this case, the
264 magnetic moments of the A_1 and A_2 atoms ($A = \text{Mn, Fe}$) are aligned parallel to each
265 other and the rest of Mn atoms remain in an antiparallel arrangement. On the other
266 hand, the calculated energies for NiTiO_3 indicate a stable G-type AFM ordering, as for
267 the pristine bulk material.¹⁸ The plotted magnetization density depicted in Figure 2
268 highlights the magnetic ground state near the vacancy, confirming the spin population
269 presented in Table 1. For MnTiO_3 and FeTiO_3 the spins of the A^{2+} neighbors are parallel
270 containing a spin-up $[\text{TiO}_5]'$ species mediating the coupling; whereas for NiTiO_3 , Ni(1)
271 and Ni(2) are antiparallel with a small amount of spin density at the Ti(2) center.

272 **Figure 2**

273 Figure 3 presents a schematic representation of the effects of the presence of V_{δ}^x
274 on the experimental G-type magnetic ordering observed for MnTiO_3 and
275 FeTiO_3 materials. Based on the analysis of the crystalline molecular orbitals, in the
276 pristine bulk, the A-O-A antiferromagnetic exchange coupling constant derives from the
277 extended 3d-2p overlap that enables virtual electron transfer between magnetic centers,
278 i.e., the mixing between transition metal 3d and oxygen 2p orbitals.⁶⁹ Both the direct
279 exchange coupling constant between occupied 3d orbitals and the super-exchange
280 coupling between A ($3d^n$) spin via $[\text{TiO}_5]'$ in the intermetallic A-O-Ti-O-A connection
281 are responsible for the distinct spin arrangement neighboring the V_{δ}^x .

282

Figure 3

283 Let us now deeply discuss the effect of oxygen vacancies on the electronic
284 properties of ATiO_3 ($A = \text{Mn, Fe, Ni}$) materials. For this purpose, atom/orbital resolved
285 density of states (DOS) and band structure profiles for defective models were
286 considered, as presented in Figures 4a-c. In addition, the theoretical results obtained for
287 the pristine bulk materials are presented in *Supporting Information* (Figures *SI-S3*) for
288 comparative purposes.

289 For MnTiO_3 (Fig. 4a), it was observed that V_{O}^x induces the creation of
290 intermediary energy levels in the band gap region of the pristine crystalline structure
291 (Fig. *SI*), narrowing the band gap from 4.48 to 2.12 eV. In addition, the nature of
292 excitation changes from direct (Γ - Γ) in the pristine material to indirect (FB- Γ) in
293 MnTiO_{3-x} , suggesting that despite the lower band gap energy, electron-hole pair
294 separation requires the coupling of phonons. Regarding the composition of both the
295 valence band (VB) and the conduction band (CB), it was noted that the lower energy
296 region of the VB is mainly composed of Mn (3d) orbitals overlapped with O(2p) states,
297 while in the vicinity of the Fermi energy level the Ti(3d) atomic orbitals are
298 predominant. On the other hand, the CB is composed primarily of empty states of Ti
299 with fewer Mn(3d) and O(2p) states. Here, it is important to point out that the states of
300 the vacancy site are present due to the treatment performed with the CRYSTAL code
301 through GHOST, where the nuclear charge is removed while the Gaussian basis sets are
302 maintained. Therefore, we can argue that the remaining electrons from V_{O}^x are trapped in
303 the $3d_{z^2}$, $3d_{yz}$ and $3d_{x^2-y^2}$ orbitals of Ti, reducing the $[\text{TiO}_5]$ cluster to $[\text{TiO}_5]'$, which
304 helps to stabilize the ferromagnetic order.

305

Figure 4

306 FeTiO₃ shows a similar pattern to MnTiO₃ regarding the distribution of atomic
307 states, where midgap states are created from V_o^x , reducing the band gap from 3.30 to
308 2.20 eV, which is indirect between FB and Γ k -points (see Fig. 4b). The major
309 differences are ascribed to the electron trapping mechanism that involves both Fe(3d)
310 and Ti(3d) orbitals. This fact can be confirmed by the larger energy difference between
311 the localized energy levels generated from the vacancy (-0.8 eV and -0.1 eV). In
312 comparison to Mn²⁺ (3d⁵), the orbital occupation for Fe²⁺ is different due to the pairing
313 of electrons in the non-degenerate a_{1g} orbital that increases the crystal field splitting
314 energy in comparison to the half-filled orbitals, which becomes higher in energy (Fig.
315 4b and S2). Then, such levels are closer in energy to the intermediary levels, enabling
316 the trapping of electrons in these orbitals, thus reducing the magnetic moment from
317 electron-pairing, as confirmed in Table 2 which shows that the spin populations of Fe²⁺
318 are more affected by V_o^x than those of Mn²⁺, once the orbital occupation is increased and
319 the local charge changes. However, in the upper part of the VB, occupied Ti(3d¹)
320 species that contribute to the overall magnetism were observed.

321 On the other hand, the antiferromagnetic order of defective NiTiO₃ was
322 confirmed by band structure and DOS analysis (see Fig. 4c). Similar to the other
323 investigated materials, a reduced indirect band gap of 2.43 eV (L- Γ) was found, as
324 compared to defect-free NiTiO₃ (5.12 eV). Combining the values for the spin
325 populations reported in Table 2 and Figure 4, it is possible to argue that the remaining
326 electrons from V_o^x are mainly trapped in empty 3d states of Ni²⁺, reducing the local
327 charge, with only a few located in Ti(3d) states. In addition, the populated Ti(3d) states
328 are closer in energy to the up- and down-spin populations, besides the similar
329 contribution indicating an additional antiferromagnetic order between these states. In

330 this case, we can suggest that the G-type AFM order of defective NiTiO₃ is stabilized
331 by a direct exchange coupling constant between half-filled Ni(3d) orbitals that is
332 negative due to the Pauli principle.

333 *3.2. Non-polar (110) surfaces*

334 The existence of oxygen defects at ATiO₃ (A = Mn, Fe, Ni) surfaces plays a
335 fundamental role in its multiferroic properties, especially in the non-polar (110) surface
336 plane which dominates the predicted morphology for MnTiO₃ as it exhibits the lowest
337 surface energy. This surface plane exhibits three symmetry-inequivalent surface oxygen
338 atoms with distinct environments. In this case, all configurations have been calculated
339 and the defect energies are shown in Table 3.

340 **Table 3**

341 It is worth noting that surface coordination is important to the energetics of
342 oxygen vacancy formation. The (110) surface plane exhibits five-fold Mn and Ti atoms,
343 but oxygen atoms in two-fold (V₁) and three-fold centers (V₂ and V₃). In all cases, it
344 was observed that two-fold oxygen atoms are more easily removed from the surface,
345 due to the reduced covalent bond number. Regarding the investigated transition metal
346 series titanates, it was noted that the defect energy is reduced from Mn to Ni in ATiO₃,
347 with the lowest formation energy found for NiTiO₃ surfaces. This fact can be attributed
348 to the covalent character associated with A-O bonds in this surface plane. Indeed, the
349 removal of a bridging two-fold oxygen atom is favored for NiTiO₃ because the
350 remaining Ni-O chemical bonds can counterbalance the electron density distribution
351 along the undercoordinated Ni and Ti atoms, in a way similar to the mechanism
352 described above which increases the local charges in bulk defective NiTiO₃ (Table 2).

353 In order to ascertain the ground-state configuration of the remaining two
354 electrons from V_O^x centers, singlet and triplet configurations were analyzed. In this case it
355 is important to point out that local changes in the antiferromagnetic ordering of ATiO_3
356 surfaces were not considered because the V_O^x center does not affect any A-O-A
357 exchange coupling. For MnTiO_3 , the remaining electrons prefer a parallel orientation,
358 which is 8.4 meV lower in energy than the singlet. In FeTiO_3 as well, there is a relative
359 energy difference of around 13.0 meV in comparison to the singlet. For NiTiO_3 a closed
360 shell solution was found to be the most stable configuration for a V_O^x center. Therefore,
361 the creation of a V_O^x center in the non-polar (110) surfaces of multiferroic ATiO_3 materials
362 can generate local ferromagnetic order inside the AFM matrix, contributing to their
363 multifunctional properties.

364 The stabilization of such ground-states is now discussed by means of the DOS
365 profiles depicted in Figure 5. For comparative purposes, the electronic atom-resolved
366 DOS for the pristine (110) surfaces can be founded in *Supporting Information* (Fig. S4).
367 An analysis of the results indicates that in all cases the V_O^x center contributes to the
368 generation of intermediary energy levels in the band gap region, thus reducing the
369 excitation energy, as observed for the defective bulk models (Fig. 4). For both
370 ferromagnetic MnTiO_3 and FeTiO_3 (110) surfaces (Fig. 5a, b), two non-degenerate
371 bands were found inside the band gap region, indicating electron localization in empty
372 3d orbitals. For MnTiO_3 , a huge contribution of Ti (3d) states was found in the vicinity
373 of the Fermi level, indicating that both electrons from V_O^x are localized in empty 3d
374 states generating magnetic parallel ordered $[\text{TiO}_4]'$ species. In addition, this state is well-
375 localized crossing the Fermi level, generating half-metallic behavior for the defective
376 MnTiO_3 (110) surfaces, where the material is a metal for the spin-up channel while

377 behaving as a semiconductor for the spin-down channel. On the other hand, for FeTiO₃,
378 both V_O^x and Ti(3d) states present similar contributions, showing that one electron
379 remains in the V_O^x with parallel spin orientation and one electron remains in the Ti (3d¹)
380 state. In an opposite way, for NiTiO₃, an almost degenerate contribution of Ti(3d) and
381 Ni(3d) states was found closer to the Fermi level, suggesting an antiparallel orientation
382 between the remaining electrons, which are located in empty β orbitals of Ni(3d⁸) and
383 Ti (3d^{1- α}).

384 **Figure 5**

385 Aiming to represent the unpaired electron density distribution in the vicinity of
386 the V_O^x in the MnTiO₃ and FeTiO₃ (110) surface planes, the magnetization density was
387 investigated from spin density isosurfaces, as depicted in Figure 6. An analysis of the
388 results shows the presence of the magnetic ground state near the vacancy, confirming
389 the spin population along the Ti atoms neighboring the vacant sites that is responsible
390 for generating the magnetic [TiO₅]' species. In particular, the Ti(3d¹) orbitals are
391 hybridized with the vacancy states; therefore, the AFM ground-state of the magnetic
392 A²⁺ cations neighboring the V_O^x remains stable for MnTiO₃ and FeTiO₃ materials, but an
393 overall magnetic contribution was attributed to spin-up reduced [TiO₅]' clusters,
394 resulting in local ferromagnetic ordering which is suitable for superior multiferroic
395 applications and spintronic technologies.

396 **Figure 6**

397 These results confirm that tuning V_O^x can effectively change the structural,
398 magnetic, and electronic degrees of freedom in ATiO₃ (A = Mn, Fe, Ni). It should be
399 emphasized that the manipulation of magnetism is achieved through the medium of the

400 Ti sites, revealing superior multiferroic properties, mainly for MnTiO_3 and FeTiO_3 ,
401 which exhibit local ferromagnetic ordering.
402

403 **4. Conclusions**

404 The energetics, structural, magnetic, and electronic properties of intrinsic neutral
405 oxygen vacancies in multiferroic $ATiO_3$ ($A = Mn, Ti, Fe$) materials were investigated
406 utilizing hybrid DFT calculations for both bulk and non-polar (110) surfaces. The
407 introduction of these defects contributes to the generation of local structural and
408 electronic disorders characterized by the existence of both $[AO_5]$ and $[TiO_5]$ clusters in
409 the bulk, as well as undercoordinated metal cations along the (110) surface plane. These
410 disorders combined to create intermediary energy levels which decreased the band gap
411 energy for all materials. Magnetic measurements point out that a local ferromagnetic
412 arrangement closer to the vacancy is lower in energy for $MnTiO_3$ and $FeTiO_3$, while
413 $NiTiO_3$ remains antiferromagnetic for both bulk and surface models. The emergence of
414 ferromagnetism for $MnTiO_3$ and $FeTiO_3$ is the result of oxygen vacancy-created
415 $[TiO_5]^{2+}(3d^1)$ defect states, which mediate the ferromagnetic coupling between the
416 localized A^{2+} spins in the bulk. For the (110) surface, the ferromagnetic order was
417 attributed to the $[TiO_4]^{2+}(3d^1)$ species that lie exposed along the surface plane increasing
418 the local magnetic moment, resulting in the particular half-metallic behavior of
419 $MnTiO_3$. Finally, a mechanism is proposed for controlling multiple order parameters of
420 $ATiO_3$ materials simultaneously by using a single parameter, V_O^x , suggesting superior
421 multiferroic orders, which make these materials suitable for multifunctional device
422 applications.

423

424 **Acknowledgments**

425 This work was supported by the State University of Ponta Grossa, University of
426 Jaume I, CAPES, PDSE-CAPES and Fundação Araucária. J. A. acknowledges the

427 financial support of the following agencies: Generalitat Valenciana for
428 PrometeoII/2014/022, Prometeo/2016/079, ACOMP/2014/270, ACOMP/2015/1202,
429 Ministerio de Economía y Competitividad, project CTQ2015-65207-P. E. Longo
430 acknowledges the financial support of FAPESP 2013/07296-2. The authors thanks to
431 Enio Longo for the support with the scientific illustrations.

432

433 **References**

- 434 1. S.-W. Cheong and M. Mostovoy, *Nature Materials*, 2007, **6**, 13.
435 2. D. I. Khomskii, *Journal of Magnetism and Magnetic Materials*, 2006, **306**, 1-8.
436 3. M. M. Vopson, *Critical Reviews in Solid State and Materials Sciences*, 2015, **40**, 223-
437 250.
438 4. N. A. Benedek and C. J. Fennie, *Journal of Physical Chemistry C*, 2013, **117**, 13339-
439 13349.
440 5. E. Claude and J. F. Craig, *Journal of Physics: Condensed Matter*, 2008, **20**, 434219.
441 6. V. E. Dmitrienko, E. N. Ovchinnikova, S. P. Collins, G. Nisbet, G. Beutier, Y. O. Kvashnin,
442 V. V. Mazurenko, A. I. Lichtenstein and M. I. Katsnelson, *Nature Physics*, 2014, **10**, 202.
443 7. T. Varga, A. Kumar, E. Vlahos, S. Denev, M. Park, S. Hong, T. Sanehira, Y. Wang, C. J.
444 Fennie, S. K. Streiffer, X. Ke, P. Schiffer, V. Gopalan and J. F. Mitchell, *Physical Review*
445 *Letters*, 2009, **103**, 047601.
446 8. A. M. Arévalo-López and J. P. Attfield, *Physical Review B*, 2013, **88**.
447 9. C. J. Fennie, *Physical review letters*, 2008, **100**, 167203.
448 10. X. Hao, Y. Xu, C. Franchini and F. Gao, *physica status solidi (b)*, 2015, **252**, 626-634.
449 11. N. Mufti, G. R. Blake, M. Mostovoy, S. Riyadi, A. A. Nugroho and T. T. M. Palstra,
450 *Physical Review B*, 2011, **83**.
451 12. T. Varga, T. C. Droubay, M. E. Bowden, R. J. Colby, S. Manandhar, V. Shutthanandan, D.
452 Hu, B. C. Kabius, E. Apra, W. A. Shelton and S. A. Chambers, *Journal of Vacuum Science*
453 *& Technology B, Nanotechnology and Microelectronics: Materials, Processing,*
454 *Measurement, and Phenomena*, 2013, **31**, 030603.
455 13. T. Varga, T. C. Droubay, L. Kovarik, M. I. Nandasiri, V. Shutthanandan, D. Hu, B. Kim, S.
456 Jeon, S. Hong, Y. Li and S. A. Chambers, *ACS applied materials & interfaces*, 2017, **9**,
457 21879-21890.
458 14. T. Varga, A. Kumar, E. Vlahos, S. Denev, M. Park, S. Hong, T. Sanehira, Y. Wang, C. J.
459 Fennie, S. K. Streiffer, X. Ke, P. Schiffer, V. Gopalan and J. F. Mitchell, *Physical review*
460 *letters*, 2009, **103**, 047601.
461 15. C. Xin, Y. Wang, Y. Sui, Y. Wang, X. Wang, K. Zhao, Z. Liu, B. Li and X. Liu, *Journal of*
462 *Alloys and Compounds*, 2014, **613**, 401-406.
463 16. R. A. P. Ribeiro, A. Camilo and S. R. de Lazaro, *Journal of Magnetism and Magnetic*
464 *Materials*, 2015, **394**, 463-469.
465 17. R. A. P. Ribeiro and S. R. de Lazaro, *RSC Advances*, 2014, **4**, 59839-59846.
466 18. R. A. P. Ribeiro, S. R. de Lazaro and C. Gatti, *RSC Adv.*, 2016, **6**, 101216-101225.
467 19. R. J. Tilley, in *Defects in Solids*, ed. R. J. Tilley, John Wiley and Sons, Hoboken, 2008,
468 DOI: doi:10.1002/9780470380758.ch1.

- 469 20. E. Albanese, C. Di Valentin and G. Pacchioni, *ACS applied materials & interfaces*, 2017,
470 9, 23212-23221.
- 471 21. H. Choi, J. D. Song, K. R. Lee and S. Kim, *Inorganic chemistry*, 2015, **54**, 3759-3765.
- 472 22. K. Inzani, T. Grande, F. Vullum-Bruer and S. M. Selbach, *The Journal of Physical
473 Chemistry C*, 2016, **120**, 8959-8968.
- 474 23. Y. Li, W. G. Schmidt and S. Sanna, *Physical Review B*, 2014, **89**.
- 475 24. H. A. Tahini, X. Tan, S. N. Lou, J. Scott, R. Amal, Y. H. Ng and S. C. Smith, *ACS applied
476 materials & interfaces*, 2016, **8**, 10911-10917.
- 477 25. F. Wang, C. Di Valentin and G. Pacchioni, *Physical Review B*, 2011, **84**.
- 478 26. Y. Zhang, J. Wang, M. P. Sahoo, T. Shimada and T. Kitamura, *Physical chemistry
479 chemical physics : PCCP*, 2015, **17**, 27136-27144.
- 480 27. E. Albanese, A. Ruiz Puigdollers and G. Pacchioni, *ACS Omega*, 2018, **3**, 5301-5307.
- 481 28. A. R. Puigdollers, F. Illas and G. Pacchioni, *The Journal of Physical Chemistry C*, 2016,
482 **120**, 4392-4402.
- 483 29. G. Pacchioni, in *Defects at Oxide Surfaces*, eds. J. Jupille and G. Thornton, Springer
484 International Publishing, Heidelberg, 1 edn., 2015, ch. 1, p. 462.
- 485 30. G. Pacchioni, *ChemPhysChem*, 2003, **4**, 1041-1047.
- 486 31. K. Yang, Y. Dai, B. Huang and Y. P. Feng, *Physical Review B*, 2010, **81**, 033202.
- 487 32. N. A. Spaldin, S.-W. Cheong and R. Ramesh, *Physics Today*, 2010, **63**, 38-43.
- 488 33. N. A. Hill, *The Journal of Physical Chemistry B*, 2000, **104**, 6694-6709.
- 489 34. T. Shimada, T. Matsui, T. Xu, K. Arisue, Y. Zhang, J. Wang and T. Kitamura, *Physical
490 Review B*, 2016, **93**.
- 491 35. T. Shimada, J. Wang, Y. Araki, M. Mrovec, C. Elsässer and T. Kitamura, *Physical Review
492 Letters*, 2015, **115**, 107202.
- 493 36. T. Xu, T. Shimada, Y. Araki, J. Wang and T. Kitamura, *Nano Letters*, 2016, **16**, 454-458.
- 494 37. T. Shimada, T. Ueda, J. Wang and T. Kitamura, *Physical Review B*, 2013, **87**.
- 495 38. A. Raeliarijaona and H. Fu, *Physical Review B*, 2017, **96**.
- 496 39. W. Li, Q. He, L. Wang, H. Zeng, J. Bowlan, L. Ling, D. A. Yarotski, W. Zhang, R. Zhao, J.
497 Dai, J. Gu, S. Shen, H. Guo, L. Pi, H. Wang, Y. Wang, I. A. Velasco-Davalos, Y. Wu, Z. Hu,
498 B. Chen, R.-W. Li, Y. Sun, K. Jin, Y. Zhang, H.-T. Chen, S. Ju, A. Ruediger, D. Shi, A. Y.
499 Borisevich and H. Yang, *Physical Review B*, 2017, **96**.
- 500 40. W. Li, R. Zhao, L. Wang, R. Tang, Y. Zhu, J. H. Lee, H. Cao, T. Cai, H. Guo, C. Wang, L.
501 Ling, L. Pi, K. Jin, Y. Zhang, H. Wang, Y. Wang, S. Ju and H. Yang, *Scientific reports*, 2013,
502 **3**, 2618.
- 503 41. S. Deng, S. Cheng, C. Xu, B. Ge, X. Sun, R. Yu, W. Duan and J. Zhu, *ACS applied materials
504 & interfaces*, 2017, **9**, 27322-27331.
- 505 42. S. Cheng, M. Li, S. Deng, S. Bao, P. Tang, W. Duan, J. Ma, C. Nan and J. Zhu, *Advanced
506 Functional Materials*, 2016, **26**, 3589-3598.
- 507 43. J. Wang, J. B. Neaton, H. Zheng, V. Nagarajan, S. B. Ogale, B. Liu, D. Viehland, V.
508 Vaithyanathan, D. G. Schlom, U. V. Waghmare, N. A. Spaldin, K. M. Rabe, M. Wuttig
509 and R. Ramesh, *Science*, 2003, **299**, 1719-1722.
- 510 44. G. Catalan and J. F. Scott, *Advanced materials*, 2009, **21**, 2463-2485.
- 511 45. T. Rojac, A. Bencan, G. Drazic, N. Sakamoto, H. Ursic, B. Jancar, G. Tavcar, M.
512 Makarovic, J. Walker, B. Malic and D. Damjanovic, *Nature Materials*, 2016, **16**, 322.
- 513 46. M. Schrade, N. Masó, A. Perejón, L. A. Pérez-Maqueda and A. R. West, *J. Mater. Chem.
514 C*, 2017, **5**, 10077-10086.
- 515 47. J. Wu, S. Mao, Z.-G. Ye, Z. Xie and L. Zheng, *Journal of Materials Chemistry*, 2010, **20**,
516 6512-6516.
- 517 48. T. R. Paudel, S. S. Jaswal and E. Y. Tsymbal, *Physical Review B*, 2012, **85**, 104409.
- 518 49. S. J. Clark and J. Robertson, *Applied Physics Letters*, 2007, **90**, 132903.

- 519 50. C. Ederer and N. A. Spaldin, *Physical Review B*, 2005, **71**, 224103.
520 51. C. Ederer and C. J. Fennie, *Journal of Physics: Condensed Matter*, 2008, **20**, 434219.
521 52. S. Sanna and W. G. Schmidt, *Journal of physics. Condensed matter : an Institute of*
522 *Physics journal*, 2017, **29**, 413001.
523 53. R. Dovesi, R. Orlando, A. Erba, C. M. Zicovich-Wilson, B. Civalleri, S. Casassa, L.
524 Maschio, M. Ferrabone, M. De La Pierre, P. D'Arco, Y. Noël, M. Causà, M. Rérat and B.
525 Kirtman, *International Journal of Quantum Chemistry*, 2014, **114**, 1287-1317.
526 54. F. Corà *, *Molecular Physics*, 2005, **103**, 2483-2496.
527 55. M. D. Towler, N. L. Allan, N. M. Harrison, V. R. Saunders, W. C. Mackrodt and E. Aprà,
528 *Physical Review B*, 1994, **50**, 5041-5054.
529 56. I. de P. R. Moreira, R. Dovesi, C. Roetti, V. R. Saunders and R. Orlando, *Physical Review*
530 *B*, 2000, **62**, 7816-7823.
531 57. C. Adamo and V. Barone, *The Journal of Chemical Physics*, 1999, **110**, 6158-6170.
532 58. R. Dovesi, A. Erba, R. Orlando, C. M. Zicovich-Wilson, B. Civalleri, L. Maschio, M. Rérat,
533 S. Casassa, J. Baima, S. Salustro and B. Kirtman, *Wiley Interdisciplinary Reviews:*
534 *Computational Molecular Science*, 2018, **0**, e1360.
535 59. R. A. P. Ribeiro, J. Andrés, E. Longo and S. R. Lazaro, *Applied Surface Science*, 2018, **452**,
536 463-472.
537 60. H. J. Monkhorst and J. D. Pack, *Physical Review B*, 1976, **13**, 5188-5192.
538 61. T. S. Bjorheim, M. Arrigoni, D. Gryaznov, E. Kotomin and J. Maier, *Physical Chemistry*
539 *Chemical Physics*, 2015, **17**, 20765-20774.
540 62. F. A. Kröger and H. J. Vink, in *Solid State Physics*, eds. F. Seitz and D. Turnbull, Academic
541 Press, 1956, vol. 3, pp. 307-435.
542 63. C. W. Raubach, Y. V. B. De Santana, M. M. Ferrer, P. G. C. Buzolin, J. R. Sambrano and E.
543 Longo, *Dalton Transactions*, 2013, **42**, 11111-11116.
544 64. R. Uarth Fassbender, T. Strelow Lilge, S. Cava, J. Andres, L. Fernando da Silva, V.
545 Roberto Mastelaro, E. Longo and M. Lucio Moreira, *Physical Chemistry Chemical*
546 *Physics*, 2015, **17**, 11341-11349.
547 65. E. Longo, E. Orhan, F. M. Pontes, C. D. Pinheiro, E. R. Leite, J. A. Varela, P. S. Pizani, T.
548 M. Boschi, F. Lanciotti, A. Beltrán and J. Andrés, *Physical Review B*, 2004, **69**, 125115.
549 66. M. M. Nakata, T. M. Mazzo, G. P. Casali, F. A. La Porta and E. Longo, *Chemical Physics*
550 *Letters*, 2015, **622**, 9-14.
551 67. S. Zhou, E. Čížmár, K. Potzger, M. Krause, G. Talut, M. Helm, J. Fassbender, S. A.
552 Zvyagin, J. Wosnitza and H. Schmidt, *Physical Review B*, 2009, **79**, 113201.
553 68. C. Di Valentin, G. Pacchioni and A. Selloni, *The Journal of Physical Chemistry C*, 2009,
554 **113**, 20543-20552.
555 69. J. B. Goodenough, *Magnetism and the chemical bond*, Interscience Publishers, 1963.

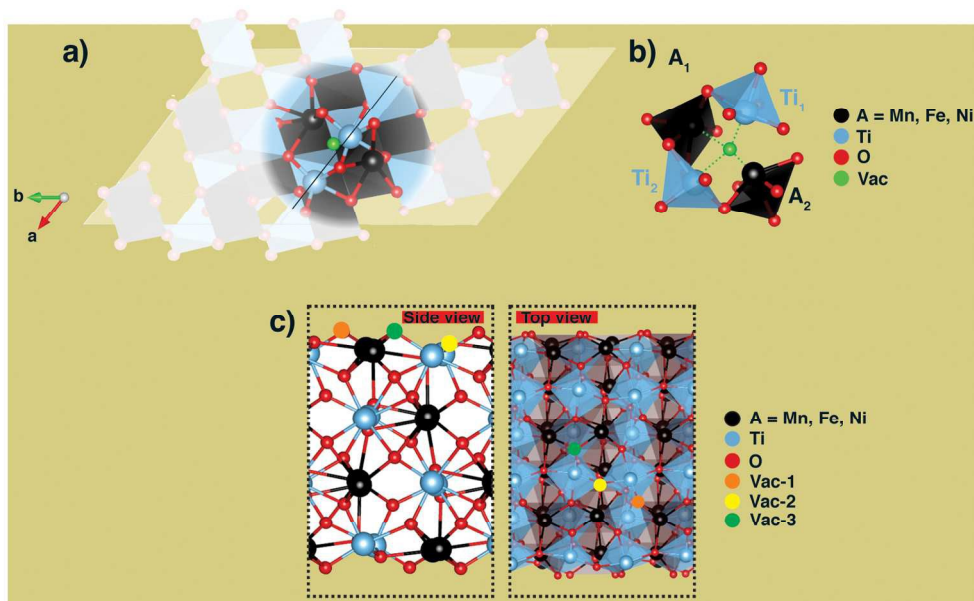


Figure 1. a) A schematic representation of the $ATiO_3$ ($A = Mn, Fe, Ni$) unit cell, where the model used to create a V_O vacancy in a $2 \times 2 \times 2$ $ATiO_3$ supercell with 80-atoms is depicted. b) Local structure in the vicinity of V_O vacancy site and the constituent clusters are highlighted. c) Side- and top-view for non-equivalent vacancy centers in (110) surface plane.

160x98mm (300 x 300 DPI)

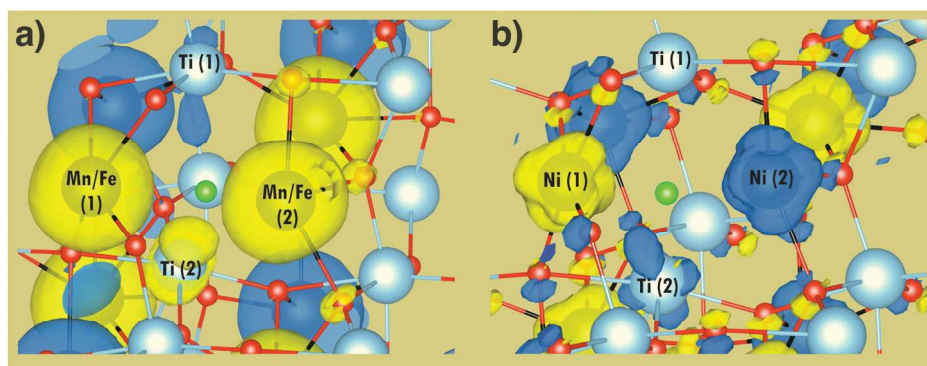


Figure 2. Spin density distribution closer to the oxygen vacancy site showing ferromagnetic ordering for MnTiO_3 and FeTiO_3 (a) and antiferromagnetic ground state for NiTiO_3 (b). Yellow and blue isosurfaces correspond to the spin-up and spin-down populations, respectively. In both cases the surface isovalue is $0.01 \text{ electron/bohr}^3$.

180x80mm (300 x 300 DPI)

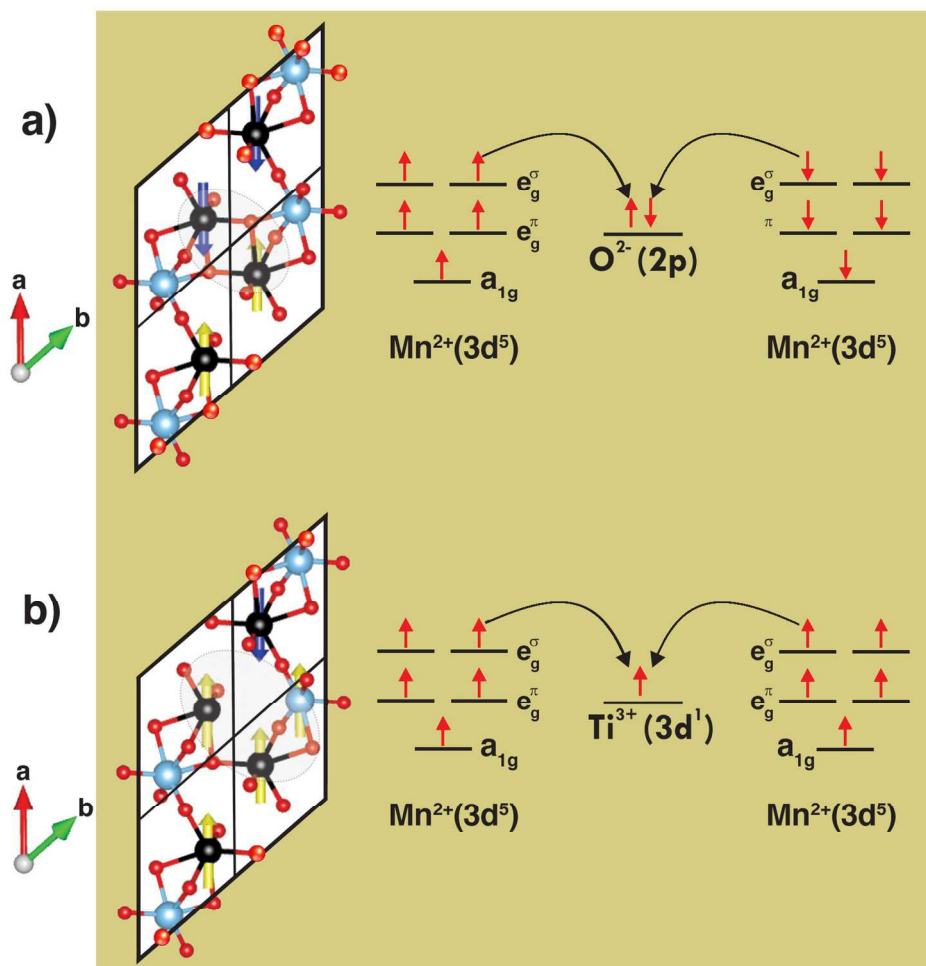


Figure 3. A schematic representation disclosing the nature of antiferromagnetic and ferromagnetic coupling constant in pristine (a) and defective (b) MnTiO₃ material. The electron transfer process mediated by oxygen and Ti³⁺ atomic states is presented in the right panel confirming the spin-orientation depicted in the left panel. A similar scheme can be sketched at the Fe²⁺. (3d⁶.) cation.

146x150mm (300 x 300 DPI)

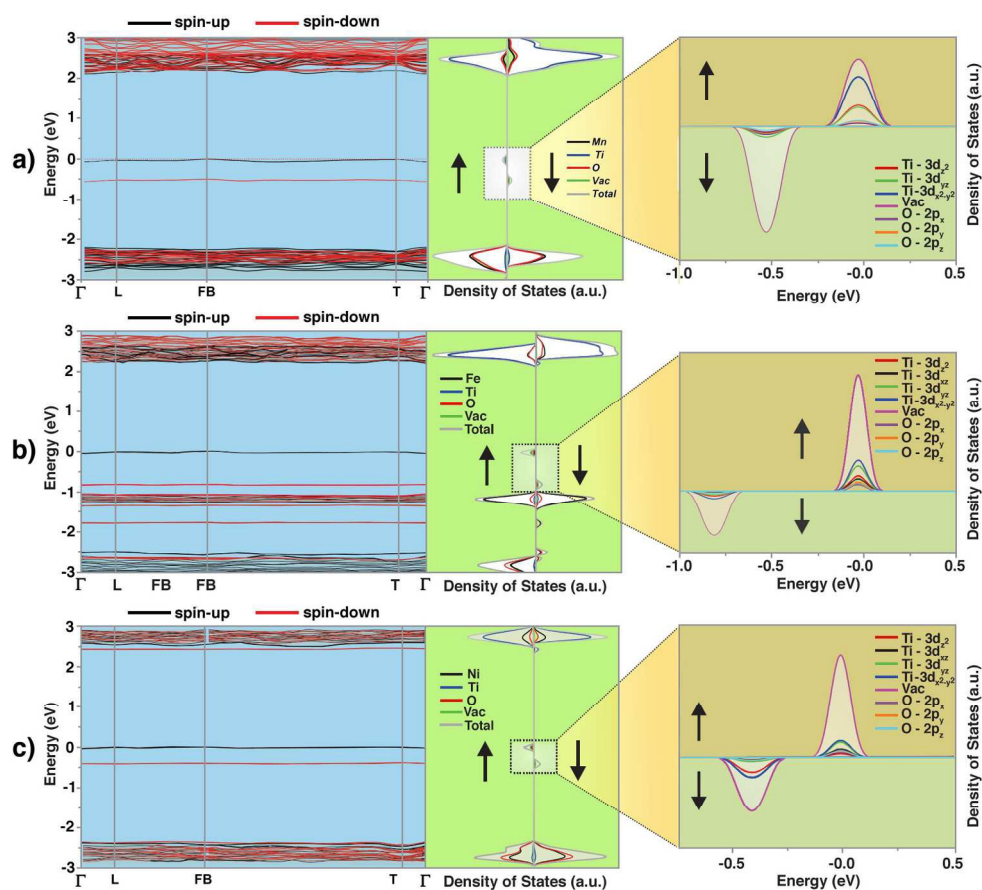


Figure 4. Band structure profile (left panel) and atom/orbital resolved DOS for a) MnTiO_3 , b) FeTiO_3 and c) NiTiO_3 materials. The inset in atom resolved DOS (middle panel) is expanded with orbital compositions (right panel). The Fermi level was set as zero in all cases.

162x147mm (300 x 300 DPI)

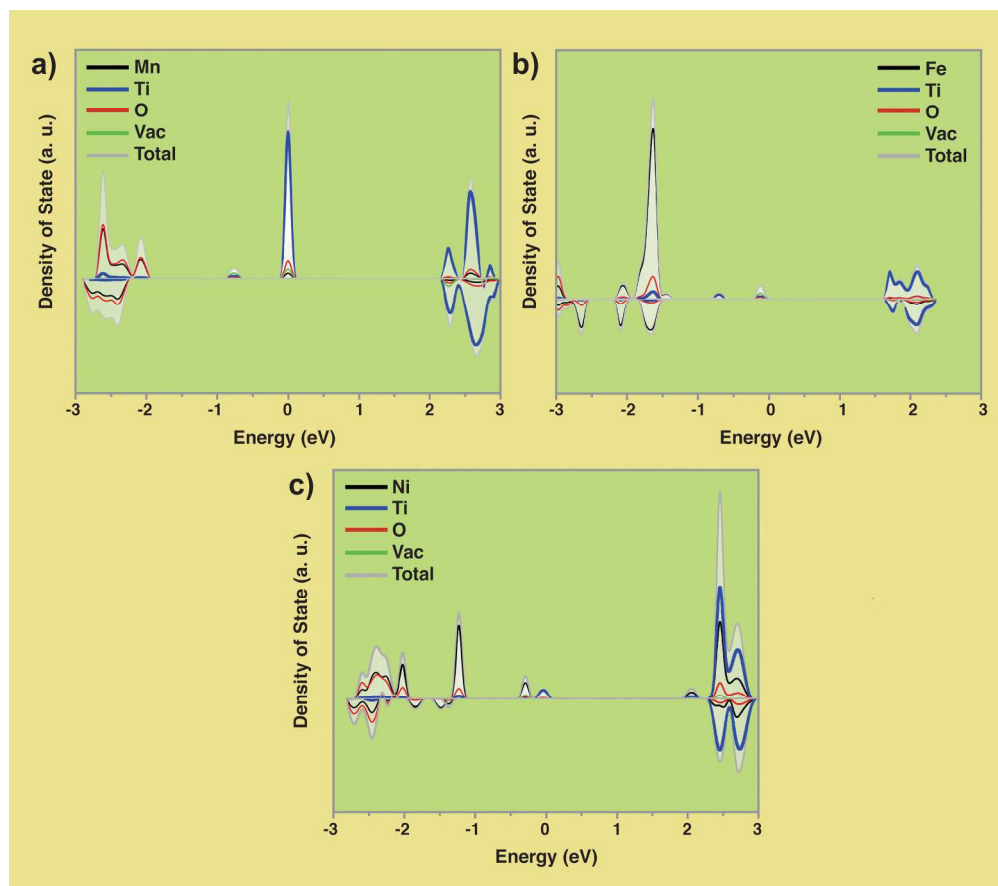


Figure 5. Atom-resolved DOS for defective a) MnTiO₃, b) FeTiO₃ and c) NiTiO₃ non-polar (110) surfaces. The Fermi level was set as zero in all cases.

189x167mm (300 x 300 DPI)

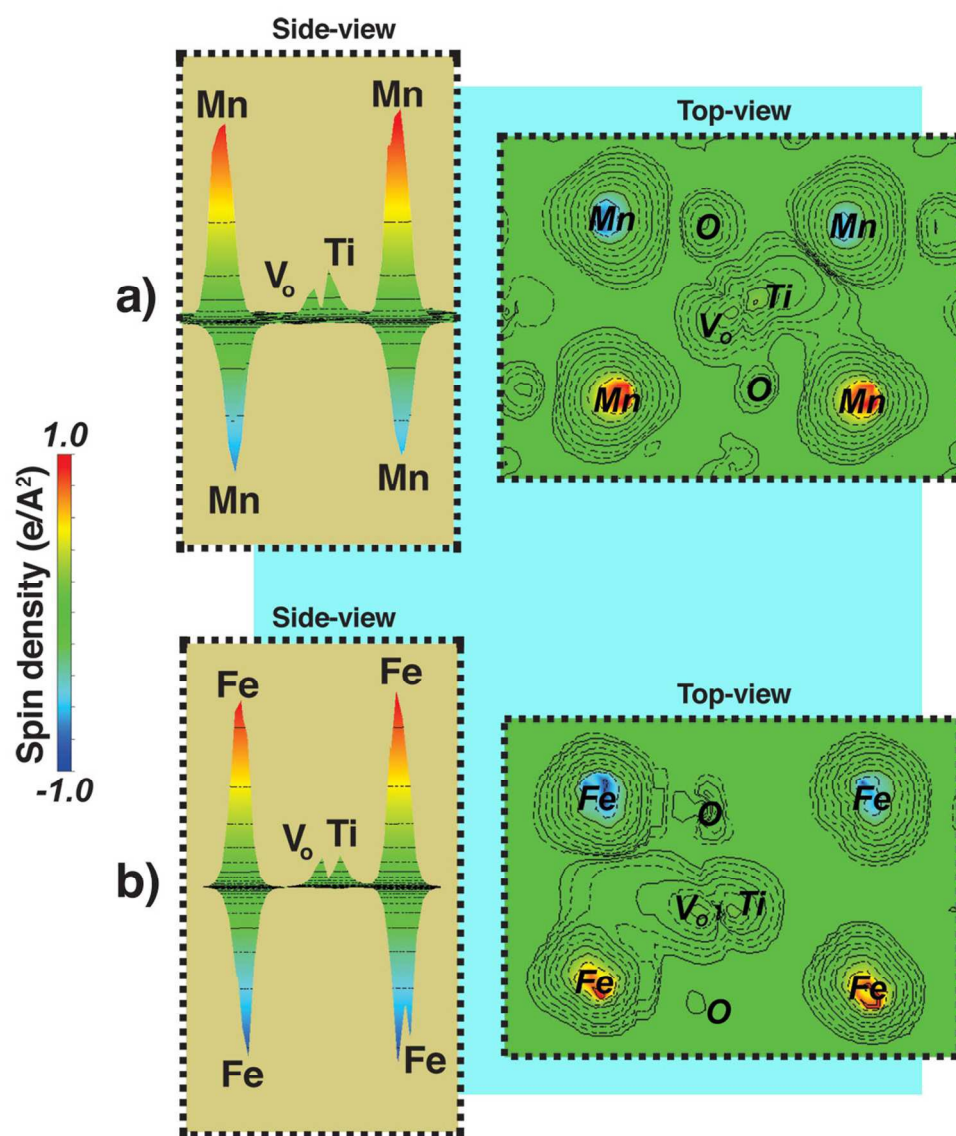


Figure 6. Spin density distribution closer to the oxygen vacancy site showing ferromagnetic ordering for (a) MnTiO_3 and (b) FeTiO_3 non-polar (110) surfaces. In both cases the surface isovalue is 0.01 electron/ bohr^3 .

101x119mm (300 x 300 DPI)

1 **A DFT investigation of the role of oxygen vacancies on the structural, electronic**
2 **and magnetic properties of ATiO₃ (A = Mn, Fe, Ni) multiferroic materials**

3 R. A. P. Ribeiro¹, E. Longo², J. Andrés^{3,*}, S. R. de Lazaro¹

4 ¹*Department of Chemistry, State University of Ponta Grossa, Av. General Carlos Cavalcanti,*
5 *4748, 84030-900, Ponta Grossa, PR, Brazil*

6 ²*CDMF-UFSCar, Universidade Federal de São Carlos, PO Box 676, 13565-905 São Carlos,*
7 *SP, Brazil*

8 ³*Department of Physical and Analytical Chemistry, University Jaume I (UJI), Castelló 12071,*
9 *Spain*

10 **Corresponding author; Email address: andres@qfa.uji.es*

11

12 **Tables**

13

14 **Table 1.** Calculated structural parameters for both pristine and oxygen deficient ATiO₃

15 (A = Mn, Fe, Ni) materials. The lattice parameters (a, b, c) and M-O bond distances (M

16 = Ti, Mn) are in Å, V in Å³ and lattice angles (α , β , γ) are in degrees. The values 1x, 2x

17 and 3x correspond to the bond multiplicity.

Structural Parameters	MnTiO ₃	MnTiO ₃ -V _O ^x	FeTiO ₃	FeTiO ₃ -V _O ^x	NiTiO ₃	NiTiO ₃ -V _O ^x
a	5.448	5.454	5.427	5.499	5.417	5.419
b		5.442		5.444		
c		5.446		5.436		
V	106.698	106.553	104.465	104.174	100.474	100.474
α	57.091	57.122	56.729	56.363	55.426	55.428
β		57.049		56.269		
γ		57.024		56.173		
Ti(1)-O	1.874 (3x)	1.871 (2x) 2.066 (1x) 2.070 (1x) 2.113 (1x)	1.866 (3x)	1.853 (1x) 1.868 (1x) 2.060 (2x) 2.112 (1x)	1.857 (3x)	1.870 (1x) 1.874 (1x) 2.055 (1x) 2.113 (1x) 2.144 (1x)
Ti(2)-O	2.091 (3x)	1.858 (1x) 1.872 (2x) 2.060 (1x) 2.099 (1x)	2.111 (3x)	1.840 (1x) 1.865 (1x) 1.899 (1x) 2.097 (1x) 2.108 (1x)	2.119 (3x)	1.823 (1x) 1.856 (1x) 1.857 (1x) 2.069 (1x) 2.088 (1x)

A(1)-O	2.115 (3x)	2.094 (1x)	2.087 (3x)	2.049 (1x)	2.041 (3x)	2.027 (1x)
		2.114 (1x)		2.063 (1x)		2.038 (1x)
		2.150 (1x)		2.124 (1x)		2.070 (1x)
		2.248 (1x)		2.189 (1x)		2.084 (1x)
		2.253 (1x)		2.341 (1x)		2.171 (1x)
A(2)-O	2.297 (3x)	2.141 (1x)	2.196 (3x)	2.069 (1x)	2.102 (3x)	2.035 (1x)
		2.142 (1x)		2.131 (1x)		2.048 (1x)
		2.235 (1x)		2.162 (1x)		2.057 (1x)
		2.297 (1x)		2.166 (1x)		2.097 (1x)
		2.431 (1x)		2.375 (1x)		2.160 (1x)

18

19

20

- 21 **Table 2.** Metal charges and spin populations (in parenthesis) obtained from Hirshfeld-I
 22 analysis for both pristine and oxygen deficient ATiO₃ (A = Mn, Fe, Ni) materials.

Metals	MnTiO ₃	MnTiO ₃ -V _O ^x	FeTiO ₃	FeTiO ₃ -V _O ^x	NiTiO ₃	NiTiO ₃ -V _O ^x
A ₁	1.92 (4.46)	1.81 (4.41)	1.93 (3.60)	1.71 (3.54)	1.91 (1.70)	1.66 (1.49)
A ₂		1.70 (4.49)		1.70 (3.63)		1.62 (-1.47)
Ti ₁	2.55 (0.0)	2.28 (-0.13)	2.54 (0.0)	2.22 (0.12)	2.55 (0.0)	2.37 (0.04)
Ti ₂		2.05 (0.36)		2.06 (0.28)		2.12 (-0.13)

23

24

25 **Table 3.** Defect formation energy (eV) for ATiO_3 (A = Mn, Fe, Ni) non-polar (110)
26 surfaces. Relative Energies (meV) between singlet (S) and triplet (T) multiplicities are
27 presented for all materials considering the most stable vacancy model. The indication in
28 parenthesis correspond to the magnetic ground-state.

Models	MnTiO₃	FeTiO₃	NiTiO₃
V ₁	5.276	4.092	3.709
V ₂	5.289	4.914	4.341
V ₃	5.635	5.059	4.803
Relative Energy	8.39 (T)	13.17 (T)	-37.38 (S)

29